Panpan Zhang, Sheng Yang, Roberto Pineda-Gómez, Bergoi Ibarlucea, Ji Ma, Martin R. Lohe, Teuku Fawzul Akbar, Larysa Baraban, Gianaurelio Cuniberti, Xinliang Feng

Electrochemically Exfoliated High-Quality 2H-MoS2 for Multiflake Thin Film Flexible Biosensors

Erstveröffentlichung in / First published in:

Small: nano micro. 2019, 15 (23), S. 1-10. Wiley Online Library. ISSN 1613-6829

DOI: https://doi.org/10.1002/smll.201901265

Final edited form was published in "Small: nano micro". 2019, 15 (23), S. 1-10. ISSN 1613-6829
https://doi.org/10.1002/smll.201901265

DOI: 10.1002/ ((please add manuscript number))
Article type: Full Paper

Electrochemically Exfoliated High-Quality 2H-MoS_2 for Multiflake Thin Film Flexible Biosensors

By *Panpan Zhang, Sheng Yang, Roberto Pineda-Gómez, Bergoi Ibarlucea, Ji Ma, Martin R. Lohe, Teuku Fawzul Akbar, Larysa Baraban*, Gianaurelio Cuniberti, and Xinliang Feng**

P. Zhang, Dr. S. Yang, J. Ma, Dr. M. R. Lohe, Prof. X. Feng
Chair for Molecular Functional Materials, Department of Chemistry and Food Chemistry, School of Science, Technische Universität Dresden, Mommsenstr. 4, 01069 Dresden, Germany.
E-mail: xinliang.feng@tu-dresden.de
R. Pineda-Gómez, Dr. B. Ibarlucea, T. F. Akbar, Dr. L. Baraban, Prof. G. Cuniberti
Max Bergman Center of Biomaterials Dresden and Institute for Materials Science, Technische Universität Dresden, 01062 Dresden, Germany.
E-mail: larysa.baraban@nano.tu-dresden.de
P. Zhang, Dr. S. Yang, J. Ma, Dr. M. R. Lohe, Dr. B. Ibarlucea, Dr. L. Baraban, Prof. G. Cuniberti, Prof. X. Feng
Center for Advancing Electronics Dresden (cfaed), Technische Universität Dresden, 01062 Dresden, Germany.

Keywords: electrochemical exfoliation, molybdenum disulfide, flexible film, Ebola biosensor

Abstract: Two-dimensional (2D) molybdenum disulfide (MoS_2) gives a new inspiration for the field of nanoelectronics, photovoltaics, and sensorics. However, the most common processing technology, e.g. liquid-phase based scalable exfoliation used for device fabrication, leads to the number of shortcomings that impede their large area production and integration. Major challenges are associated with the small size and low concentration of MoS_2 flakes, as well as insufficient control over their physical properties, e.g. internal heterogeneity of the metallic and semiconducting phases. Here we demonstrate that large semiconducting MoS_2 sheets (with dimensions up to 50 μm)

Final edited form was published in "Small: nano micro". 2019, 15 (23), S. 1-10. ISSN 1613-6829
https://doi.org/10.1002/smll.201901265

can be obtained by a facile cathodic exfoliation approach in non-aqueous electrolyte. The synthetic process avoids surface oxidation thus preserving the MoS_2 sheets with intact crystalline structure. We further demonstrate at the proof-of-concept level a solution-processed large area (60 × 60 μm) flexible Ebola biosensor, based on a MoS_2 thin film (6 μm thickness) fabricated via restacking of the multiple flakes on the polyimide substrate. The experimental results reveal a low detection limit (in fM-pM range) of the fabricated sensor devices. We are confident that the presented exfoliation method opens up new opportunities for fabrication of large arrays of multifunctional biomedical devices based on novel 2D materials.

1. Introduction

The great success of graphene research has motivated widespread interests in semiconducting 2D materials such as transition metal dichalcogenides (TMDs), which present indirect bandgaps in the range of 1.0-2.0 eV and are suitable for electronic devices.[1] Molybdenum disulfide (MoS_2) is the one of the most explored TMDs, ideal for new generation electronics,[2] optoelectronics,[3] and topological insulators.[4] Several examples of applications can be found where MoS_2 thin films are used, such as sensors,[5] energy storage[6] or flexible electronics.[7] Thus, a method to prepare highly concentrated and stable dispersions of excellent quality semiconducting TMDs materials is essential in order to achieve solution-processed, inexpensive, large area high performance devices.

However, exfoliated MoS_2 flakes exhibit heterogeneous properties, depending on

Final edited form was published in "Small: nano micro". 2019, 15 (23), S. 1-10. ISSN 1613-6829
https://doi.org/10.1002/smll.201901265

their thickness, lattice structures as well as chemical composition. The synthetic methods are thus critically important, in order to access their intact properties. Considerable progress have been achieved to overcome the weak interlayer interactions to produce mono- or few-layer MoS_2 using micromechanical cleavage,[2, 8] chemical intercalation,[9] and ultrasound-promoted shear exfoliation.[10] While micromechanical cleavage is able to obtain pristine MoS_2 flakes with very limited yield, the chemical routes using harsh *tert*-butylithium-mediated intercalation are able to produce single-layer MoS_2 flakes with large quantity. However, the lithium intercalation converts MoS_2 from pristine semiconducting 2H phase to metallic 1T phase. Beyond that, liquid-phase exfoliation with suitable solvents (*e.g. N*-methyl-2-pyrrolidone (NMP)) offers macroscopic quantity of 2H-MoS_2 flakes.[11] Nonetheless, it requires long-last agitation (*e.g.* 23 h) and delivers low exfoliation yields (~40%) as well as small sheet sizes (less than 1 μm).[12] By now, it remains a great challenge to prepare large sheet size, high-quality 2H-MoS_2 flakes with high yield.

Herein, we demonstrated a novel scalable method to prepare high-quality 2H-MoS_2 flakes by cathodic exfoliation in organic electrolyte. Especially, the intercalation of tetra-*n*-butyl-ammonium cations in bulk MoS_2 benefits to fast exfoliation within 1 hour, high yield of 70% and large-sized flakes up to 50 μm. The method is appealing to obtain high quality multiflake films with no throughput limitations for the variety of electronic applications abovementioned. As a first application, we fabricated the large-area biosensor, developed by a restacking the 2H-MoS_2 flakes into thin film on the flexible polyimide support. Developed sensor array revealed low detection limit of VP40 matrix

Final edited form was published in "Small: nano micro". 2019, 15 (23), S. 1-10. ISSN 1613-6829
https://doi.org/10.1002/smll.201901265

protein from Ebola virus down to picomolar levels as well as excellent flexibility even after bending down to 1 mm radius. The results showed that this exfoliation approach could be appropriate in the future for rapid fabrication of 2D materials based arrays of electronic devices, *e.g.* for light weight biosensors to be used in remote areas or in case of emergency of fatal disease spread.

2. Results and Discussion

2.1. Electrochemical Exfoliation of MoS_2 Crystal

In this study, electric current is used as a main driving force to push ions or charged molecules into the interlayers of natural MoS_2 crystal. **Figure 1**a schematically illustrates the experimental setup for the electrochemical exfoliation, where a piece of MoS_2 crystal, a Pt foil, and 0.1 M tetra-*n*-butylammonium bisulfate (TBA▪HSO_4) in propylene carbonate were used as a working electrode, a counter electrode, and an electrolyte, respectively. TBA▪HSO_4 is highly soluble in a wide cast of organic solvents, providing great freedom for the electrolyte design. Because the size of TBA^+ cation (0.85 nm) is generally greater than the interlayer spacing of MoS_2 layers (0.615 nm),[13] the expansion at the boundaries of MoS_2 crystal is necessary to allow the intercalation of large TBA^+ cations. A low positive bias of +5 V was applied on the MoS_2 foils for 5 min, to intercalate small anions (SO_4^{2-}), for the subsequent intercalation by cationic TBA^+. Once switching to -5 V, massive gas bubbles were observed, owing to the reduction of the intercalated SO_4^{2-} through chemical reactions: $SO_4^{2-} + 4H^+ + 2e^- \rightarrow 2H_2O + SO_2\uparrow$. The MoS_2 crystal began to swell, dissociated into small pieces and

Final edited form was published in "Small: nano micro". 2019, 15 (23), S. 1-10. ISSN 1613-6829
https://doi.org/10.1002/smll.201901265

suspend in the electrolyte, as shown in Figure S1 and Movie S1, Supporting Information. The efficient expansion and exfoliation were further confirmed by optical images (Figure 1b). In order to access the optimal experimental conditions, working bias was carefully manipulated (Figure S2-4, Supporting Information). A moderate potential of -5 V was applied for 1 h to achieve efficient exfoliation.

The mechanism of electrochemical exfoliation of natural MoS_2 crystal is proposed in Figure 1d. Thanks to the variable diameters of TBA^+ cations (0.47 nm for flattened configuration and 0.89 nm for tetrahedral configuration),[14] the insertion of TBA^+ cations enables the expansion of the interlayer spacing of MoS_2 foil to a maximum gallery of 0.89 nm. Afterwards, the migration and reduction of H^+ produce hydrogen bubbles, further enlarging the gaps between adjacent layers, which is essential to overcome the van der Waals interactions.

$$TBA{\cdot}HSO_4 \leftrightarrow TBA^+ + HSO_4^- \quad (1)$$

$$HSO_4^- \leftrightarrow SO_4^{2-} + H^+ \quad (2)$$

$$2H^+ + 2\,e \rightarrow H_2\uparrow \quad (3)$$

The cathodic reduction can possibly transform TBA^+ into other species.[15] The large volume expansion combined with gas release overcome the weak interactions between MoS_2 layers.

$$(n\text{Butyl})_4N^+ + e \rightarrow (n\text{Butyl})_4N{\cdot} \quad (4)$$

$$(n\text{Butyl})_4N \bullet \rightarrow n\text{Butyl}{\cdot} + (n\text{Butyl})_3N \quad (5)$$

$$n\text{Butyl}{\cdot} + e \rightarrow n\text{Butyl}^- \quad (6)$$

To validate it, the morphologies of a MoS_2 electrode at different time periods (0-10

Final edited form was published in "Small: nano micro". 2019, 15 (23), S. 1-10. ISSN 1613-6829
https://doi.org/10.1002/smll.201901265

min) were monitored by scanning electron microscopy (SEM) (Figure 1e-g, Figure S5, Supporting Information). The well-defined edges were evolved into disordered porous structure, which strongly supports our hypothesis that during the electrochemical process, grain boundaries of the MoS_2 electrode open up to promote cationic intercalation, leading to the exfoliation of MoS_2 flakes. Based on the mass ratio between dispersed sheets to the starting precursor, the total exfoliation yield is about 70 %, surpassing that of liquid exfoliation methods (~40 %). The exfoliated MoS_2 flakes were collected using vacuum filtration and washed repeatedly with water/ethanol, then redispersed in propylene carbonate to obtain a homogeneous dispersion (Figure 1c). The concentration of obtained MoS_2 dispersions was in a range of 0.1-0.5 mg mL^{-1}. In addition, by tailoring the sizes of electrochemical cell and MoS_2 foils, this method is ready for scaled-up production, which is one of the major advantages in comparison to micromechanical cleavage,[2, 8] chemical intercalation,[9] and ultrasound-promoted shear exfoliation,[10-12] that generally lead to limited yield (<3 %), poor structural integrity and/or small sheet sizes (sub 1 μm) (Table S1, Supporting Information).

2.2. Characterization of High-Quality MoS_2

Additional centrifuge process was used to selectively separate the flakes and remove the unexfoliated thick materials (Figure S6, Supporting Information). The small flakes (sub 1 μm) were commonly observed in the supernatant, whereas large flakes (more than 5 μm) showed up frequently in the middle of the dispersion. The mixed dispersion was subsequently transferred onto Si/SiO_2 substrates by spray coating. **Figure 2**a shows

Final edited form was published in "Small: nano micro". 2019, 15 (23), S. 1-10. ISSN 1613-6829
https://doi.org/10.1002/smll.201901265

the SEM images of exfoliated MoS_2 flakes with a lateral dimension between 10 and 50 μm. In addition, transmission electron microscopy (TEM, Figure 2b) of few-layered exfoliated MoS_2 flakes exhibit the transparent morphology and the folded edge. High-resolution TEM (HR-TEM, Figure 2c) images confirm the distinct crystal lattice and hexagonal lattice structure of MoS_2 flakes, suggesting the undamaged process of electrochemical exfoliation. The well-defined lattice space of 0.17 and 0.28 nm were observed, corresponding to (110) and (100) plane. The selected area electron diffraction (SAED) patterns (insets of Figure 2b,c) indicate hexagonal symmetry of the atomic arrangement in 2H-MoS_2 and that individual sheets consist of a single crystal domain, implying that the as-exfoliated MoS_2 flakes inherited the nature of high-quality.[16]

X-ray photoelectron spectroscopy (XPS) spectra of the exfoliated sample display the bands of Mo 3d and S 2p, as the main characteristic of MoS_2 (Figure S7, Supporting Information). In detail, the Mo 3d shows two peaks at 232.5 (Mo $3d_{3/2}$) and 229.5 eV (Mo $3d_{5/2}$), while the S 2p is located at 163.5 (S $2p_{1/2}$) and 162.0 eV (S $2p_{3/2}$), as the key feature of 2H-MoS_2. Atomic force microscopy (AFM, Figure 2d,e) measurements from small flakes show that the thicknesses are 3.9−6.7 nm, corresponding to 6−10 layers. As an additional benefit, such high-quality MoS_2 sheets are highly solution-processable for various applications. Subsequently, a MoS_2 thin film (ca. 1 μm thick) was fabricated with the stable dispersion by applying vacuum filtration through a polytetrafluoroethylene (PTFE) membrane (inset of Figure 2f). Top-view SEM and corresponding energy-dispersive spectroscopy (EDS) elemental mapping show large-

Final edited form was published in "Small: nano micro". 2019, 15 (23), S. 1-10. ISSN 1613-6829
https://doi.org/10.1002/smll.201901265

area uniformity and continuity of the MoS_2 thin film (Figure 2f, Figure S8, Supporting Information).

2.3. Fabrication of Ebola Biosensors

We further demonstrated the excellent performance of the exfoliated MoS_2 flakes as electronic biosensors fabricated using multiple interconnecting flakes contacted between gold electrodes, and incorporating specific antibodies as receptors for VP40 protein from Ebola (see concept **Figure 3**a). The electrical response of the device has been tested at the flexible polyimide support and used as a light-weight biosensor. For the fabrication, MoS_2 flakes were deposited from an ethanol dispersion onto a flexible polyimide support following a simple transfer procedure[17], shown in Figure S9 (Supporting Information). The hydrophobic properties of MoS_2 and the surface tension of water allows the floatability of MoS_2 flakes inside the area defined by polydimethylsiloxane (PDMS) window,[18] forming a compact thin film (Figure 3b-i) and then assembled into the device. The square shape area (60 × 60 μm) between the electrodes was used for antibody immobilization and antigen sensing. The chip, containing up to 12 working sensors, is shown in Figure 3b-ii, with a magnified image in Figure 3b-iii. An AFM measurement indicated a film thickness of up to 5-6 μm (Figure 3b-iv). The resultant devices were used for a bending test under several bending radii between 14 mm and 1 mm (see bended chip in Figure 3c). The as-prepared devices displayed Schottky junction characteristics with an ON current (I_{ON}) of ~5×10^{-5} A and an OFF current (I_{OFF}) of ~1×10^{-11} A (Figure 3d, red line).

Final edited form was published in "Small: nano micro". 2019, 15 (23), S. 1-10. ISSN 1613-6829
https://doi.org/10.1002/smll.201901265

Bending analysis was performed by attaching the carrier foil to cylindrical objects in range of 14 mm down to 1 mm radius, far below the curvature required in external biomonitoring applications.[19] As depicted in Figure 3d, I_{ON} was maintained at the initial level, with only minor decrease with bending radii at 14 mm (20 µA) and 8 mm (5 µA). An observed gradual degradation with further increasing bending radii from 6, 4.5 to 2 mm, the device still worked with ca. 0.1 µA current retention. SEM images showed how deterioration was caused by detachment and loss of flakes from the intercalating conducting path (blue and green colored marks in Figure 3e). As indicated in the highlighted area, a conductive pathway between the four electrodes still existed after 8 mm bending radius, and remained even after 1mm bending.

Apart from the static mechanical characterization, we perform dynamic bending tests of the flexible devices in order to observe the degradation of their performance after 100 consecutive bending cycles (see Figure 3f,g). In order to realize these measurements, the polyimide foils with the fabricated devices were repeatedly bent at the cylinder with the diameter of 8 mm (Figure 3f). We do not observe visible degradation of the device performance even after 100 bending-unbending cycles, which is reflected in the practically unchanged *I-V* characteristics (Figure 3g).

Remarkably, the results obtained using this relatively cheap and simple fabrication method, are comparable or even outperform some of the recent reported flexible electrical devices based either on single MoS_2 flakes (2.2 - 10 mm)[20] or chemical vapor deposition (CVD) grown (9 - 14 mm)[21], and others fabricated in polyimide supports

Final edited form was published in "Small: nano micro". 2019, 15 (23), S. 1-10. ISSN 1613-6829
https://doi.org/10.1002/smll.201901265

using various materials such as organic films (28 mm)[19], silicon nanowires (7.5 mm)[22] graphene (4 mm)[23], or ZnO nanostructures (9 mm)[24].

Antibodies against VP40 were immobilized on MoS_2 to confer the sensor with the required specificity (**Figure 4**a). The immobilization was realized using thiol-containing 11-mercaptoundecanoic acid (11-MUA) as cross-linker, anchored to the boundaries or sulphur vacancies,[25] and connected with antibody through carbodiimide chemistry. A colorimetric confirmation using toluidine blue O (TBO) is provided in the Supporting Information.[26] Any remaining available binding point at the surface after antibody immobilization was blocked by a further incubation in 0.5 mg mL^{-1} bovine serum albumin (BSA).

The biosensing performance of the device was evaluated by comparing the output characteristics in dry state before and after the incubation of solutions upon increasing VP40 concentrations (fM-pM range for sample #1). 20 µL PBS with target protein were deposited on the sensing area and incubated for 30 min. Then, PBS was used for rinsing, followed by a rinse using 10-fold diluted PBS to remove excess of salts. The results were compared with those obtained using Staphylococcal enterotoxin B (SEB) as analyte, which shows initial symptoms similar to Ebola disease if ingested. Additionally, a control experiment was done detecting VP40 with a sensor lacking antibodies. The current at 2 V increased after exposure to increasing VP40 concentration in the femtomolar range with saturation at picomolar levels (Figure 4b,c). When using sensors with lower current due to a lower amount of flakes at the sensing area (sample #2) the detection range shifted to pico- and nanomolar range (Figure 4d),

Final edited form was published in "Small: nano micro". 2019, 15 (23), S. 1-10. ISSN 1613-6829
https://doi.org/10.1002/smll.201901265

which we attribute to the presence of a lower amount of MoS_2 flakes occupying the same area, as reflected by a lower current level (10^{-8} A), and therefore less anchoring points for antibodies, resulting in a low probability of interaction with target protein. After dissociation of the antibody-antigen complex by incubation in a 10 mM glycine-based regeneration buffer (pH = 2) the signal was recovered, allowing to repeat the VP40 detection again (Figure 4e). After the regeneration, the same tendency in the signal change in the pico- and nanomolar analyte concentration range could be repeated.[27]

Since MoS_2 is a semiconductor material, the sensing mechanism in the absence of a gate electrode can be explained as molecular gating caused by the attached VP40 proteins, which modulate the carrier density. The biosensors recognize binding events of charged or polar biological species, because the electrostatic interaction between biomolecules and gate dielectric or channel gives rise to conductance modulation.[28] Under such conditions, tiny variation of current can be detected when using semiconducting MoS_2 as active layers, rather than metallic MoS_2. Finally, fetal bovine serum with spiked VP40 was employed as a more relevant medium for Ebola testing. A signal change was observed in the same concentration range, although the tendency was opposite to the buffer system. Incubations in serum without spiked analyte protein, both before and after the experiment, did not show any tendency, indicating that it must be related to the presence of VP40. This phenomenon, which could be related to interaction of the VP40 with other molecules leading to a change on the net charge of the analyte needs further studies.

Final edited form was published in "Small: nano micro". 2019, 15 (23), S. 1-10. ISSN 1613-6829
https://doi.org/10.1002/smll.201901265

The biosensing response fits the picomolar antigen sensitivity levels expected for rapid Ebola diagnosis in point-of-care situations.[29] The results also improve by several orders of magnitude those obtained by traditional methods such as the enzyme-linked immunosorbent assay and are similar to recent nanosensors with a more complicated fabrication process,[30] offering a promising alternative for fast and low-cost delivery and use in emergency situations or in remote areas. Comparable detection levels as well as sensing areas (**Table 1**) were obtained by other recent electrical biosensors based on MoS_2 with *more complex* fabrication methodology, *not flexible*, or *not tested down to such low bending radius* (1 mm). The biosensor also shows remarkable performance with similar or better limit of detection compared to other Ebola detection techniques, showing no particular drawbacks such as necessity of special safety facilities, labeling, or difficulties for miniaturization (see Table S2, Supporting Information). Certain nonspecific adsorption was observed when no antibodies were present (Figure 4c), as well as a slight signal decrease when a non-specific antigen (SEB) was incubated. The latter could be attributed to a small deterioration of the performance of the device but with no protein attachment.

One of the main advantages of MoS_2 in terms of biosensing applications is that, in contrast to other 2D materials such as graphene, strong covalent bonds can be directly created on its sulphur vacancies using thiolated molecules,[25] without needing to follow preliminary oxidation steps to create functional groups[31] or relying on non-covalent interactions[32] for the incorporation of bioreceptors. Despite most of the sulphur vacancies theoretically exist at the edges of the MoS_2 flakes, the multiflake structure of

Final edited form was published in "Small: nano micro". 2019, 15 (23), S. 1-10. ISSN 1613-6829
https://doi.org/10.1002/smll.201901265

the sensing area allows to present a density of binding sites high enough to generate current changes in the observed response range in femto- and picomolar concentrations. Additional antibody presence by strong adsorption on areas without imperfections due to the hydrophobic nature of MoS_2 cannot also be discarded.[28b] An estimated maximum amount of 2×10^8 antibodies in the total MoS_2 sensing area of 1×10^{10} nm^2 would allow detecting the 2.1×10^7 antigen molecules settled above the same area when the lowest tested concentration (2 fM) was incubated, and still leave free binding sites to reach a saturation at 2 pM concentration (2.4×10^{10} antigens settled).

3. Conclusions

In summary, we have demonstrated the efficient exfoliation of natural MoS_2 crystal based on an electrochemical strategy, producing MoS_2 flakes with a high yield (ca. 70%) and large flakes up to 50 μm, thanks to the intercalation of tetra-*n*-butyl-ammonium cations in bulk MoS_2. The exfoliated flakes exhibit intact crystallinity and high structural integrity. Further, the resultant MoS_2 compact films were successfully biofunctionalized with antibodies against VP40. The as-prepared biosensor withstands severe mechanical deformations. In addition, the device shows remarkable analytic performance with the limit of detection of the target VP40 molecules down to femtomolar levels and surface regeneration capability. A proper electrode passivation and the incorporation of a gate terminal would allow exploiting the semiconducting properties of the MoS_2 as a field-effect transistor, an electronic format that provides further application possibilities like interfacing and measuring directly in liquid

Final edited form was published in "Small: nano micro". 2019, 15 (23), S. 1-10. ISSN 1613-6829
https://doi.org/10.1002/smll.201901265

environments (*e.g.* analysis of biological dynamics[33] or nanoliter compartments[34]) or photodetection[35]. Therefore, this work not only provides a simple, efficient and scalable approach to prepare and functionalize high-quality MoS_2 flakes for high-performance biomedical devices, but also contributes to the widespread potential in other multifunctional applications.

4. Experimental Section

Synthesis of Electrochemically Exfoliated MoS_2 Flakes: The electrochemically exfoliated MoS_2 flakes were produced as follows. Typically, the natural MoS_2 crystal, a Pt foil, and 0.1 M tetra-*n*-butylammonium bisulfate (TBA▪HSO_4) in propylene carbonate (PC) were acted as working electrode, counter electrode, and electrolyte, respectively. The distance between the natural MoS_2 crystal and the Pt electrode was ~2 cm and was kept constant during the electrochemical process. The electrochemical exfoliation of MoS_2 crystal was conducted at different conditions for a certain time. After that, the exfoliated MoS_2 flakes were collected on a polytetrafluoroethylene (PTFE) membrane filter with 0.2-μm pore size by vacuum filtration, and washed several times with ethanol and deionized water. The resultant sample was dispersed in PC by sonication for 1 h. The dispersion was kept for 24 h, and the supernatant dispersion of MoS_2 flakes was directly used for further functionalization.

Device Fabrication: The fabrication process (depicted in Figure S8) starts with the substrate material polyimide (DuPont™ Kapton® HN500, 127 μm thickness). Polyimide is a lightweight, flexible material that is resistant to relative high

Final edited form was published in "Small: nano micro". 2019, 15 (23), S. 1-10. ISSN 1613-6829
https://doi.org/10.1002/smll.201901265

temperatures (0.10% shrinkage at 200°C according to provider) and chemically inert.[36] Therefore, it is broadly employed in electronics for producing flexible cables, as an insulator film on magnet wire and for medical tubing[37] and as a support for nanoscale sensors.[22, 38]

Polyimide film is cut in a square of 35 × 35 mm^2. After, the substrate was cleaned with acetone, ethanol, and deionized water using ultrasonic bath during 2 minutes each to get rid of some particles at its surface. Gold electrodes were defined following a standard photolithography process (Figure S8-i). A layer of positive photoresist (MICROPOSIT™ S1828™ G2, Dow® Electronic materials) was placed using spin coating. The setup used for the spin coating process was 4000 rpm with an acceleration of 4000 rpm/s during 1 minute. The mask with the desired electrode layout was aligned with the substrate and a first UV-lithography took place, for 10 seconds. After that, the exposed structures were developed (Developer bath AZ 726 MIF, AZ Electronic Materials) for one minute and rinsed in deionized water getting rid of residues. The fabrication process continued with the deposition of gold for the electrodes. A pre-adhesive layer of 3 nm of chromium was thermally evaporated on top of the polyimide substrate. The metal film thickness was approximated measuring the deposition rate with quartz crystal deposition control. A layer of 50 nm of gold was deposited on top of the chromium layer by implementing the same thermal evaporation method. Following lift off was carried out immersing the sample for 5 minutes in acetone followed by ultrasonication for 1 minute and a second bath of acetone, getting rid of the all the photoresist.

Final edited form was published in "Small: nano micro". 2019, 15 (23), S. 1-10. ISSN 1613-6829
https://doi.org/10.1002/smll.201901265

Subsequently a second step of lithography was used to define the channel area (Figure S8-ii). The MoS_2 solution was deposited using a polydimethyl siloxane (PDMS) window which was tightly bound to the polyimide substrate (Figure S8-iii,iv). This material restricted the area of the deposited MoS_2 enhancing the usage of it. Big multi-layered MoS_2 nanosheets (size: 5-30 μm, thickness: few tens of nanometers) were deposited using water as an agent to distribute the material in a uniform way. The surface tension of the water allowed to form a large uniform MoS_2 layer on top of it, without sinking or dispersing. The materials were placed on top of a heating plate and a temperature of 70 ºC was used to evaporate the water. The MoS_2 subsequently was deposited over the underlying materials (Figure S8-v), finishing the fabrication process by removing the PDMS and photoresist (Figure S8-vi).

The method here presented, does not require of special conditions such as vacuum, a temperature more than 70ºC, or an indirect transfer; hence it avoids the use of additional elements and fabrication steps decreasing contaminants and helping to keep its original properties thus enhancing its viability for scalable production. The hydrophobic properties of MoS_2 and the surface tension of water allows the floatability of MoS_2 flakes on water,[18] forming a compact thin film, which will be softly precipitated onto the surface through evaporation of the water underneath. The capability to perform as a flexible device allows its handling under conditions were a manipulation and handling might impede a possible test under physically demanding circumstances.

Bending Test: Mechanical performance of the sensor was tested in the initial conditions, as fabricated (red color curve in Figure 3d) as well as under bending

Final edited form was published in "Small: nano micro". 2019, 15 (23), S. 1-10. ISSN 1613-6829
https://doi.org/10.1002/smll.201901265

conditions at different radii, from 14 mm down to 1 mm (light to dark green curves, Figure 3d). The device was placed in the corresponding curved surface according to the desired radius (bottom panels in Figure 3c), and the electrodes were contacted with the help of micropositioners. Source-to-drain voltage (V_{SD}) was swept and the resulting current was measured with a 2604B Keithley source meter (Keithley Instruments), obtaining the output characteristics of the device. In the case of 1 mm radius, it was no more possible to directly contact the electrodes with the positioners, therefore the device was measured after the bending.

Further, we performed dynamic bending tests of the flexible devices in order to observe the degradation of their performance after 10 bending cycles consisting on 10 bending each (total of 100 bending events) (see Figure 3f,g). In order to realize these measurements, the polyimide foils with the fabricated devices were consecutively bended at a cylindrical tool of 8 mm radius and the foil was repeatedly bent.

MoS_2 Biofunctionalization and Biosensing: Antibodies against VP40 were immobilized on MoS_2 to confer the sensor with the required specificity. The followed steps are depicted in Figure 4a. The immobilization was done using thiol containing 11-mercaptoundecanoic acid (11-MUA) as cross-linker. First, the sensor was immersed overnight in an absolute ethanol solution containing 10 mM 11-MUA. The thiol group of this molecule bonded on the sulphur vacancies at the MoS_2 imperfections,[25] leaving exposed its carboxyl end. This group was activated by 15 min. incubation in a phosphate buffered saline (PBS) solution containing 5 mM N-Hydroxysuccinimid and 10 mM N-(3-Dimethylaminopropyl)-N′-ethylcarbodiimide hydrochloride. After

Final edited form was published in "Small: nano micro". 2019, 15 (23), S. 1-10. ISSN 1613-6829
https://doi.org/10.1002/smll.201901265

rinsing with PBS, the antibody was incubated on the MoS_2 surface for 1 h (0.01 mg mL^{-1} in PBS). Any remaining available binding point at the surface was blocked by a further incubation in 0.5 mg mL^{-1} bovine serum albumin (BSA). After a final thorough rinse with PBS, the biosensor was ready to use.

The 11-MUA immobilization was confirmed by colorimetric analysis using toluidine blue O (TBO) as indicator.[26a] Briefly, 2 cm^2 samples completely covered by MoS_2 and modified with 11-MUA were immersed overnight in deionized water with 0.15 mg mL^{-1} TBO and adjusted to pH = 10 using hydrochloric acid. In alkaline pH the positively charged TBO binds electrostatically the negatively charged carboxyl groups from the 11-MUA in a 1:1 ratio. After rinsing with deionized water at the same pH to remove the loosely attached TBO, 1 mL acetic acid 50% was deposited on top of the samples for 15 min in order to extract the bonded dye. The light absorbance of the extraction solution was recorded by spectrophotometry and the absorbance peak of the TBO was measured at 633 nm. The absorbance spectra can be seen in Figure S10. The surface density could be calculated by comparing the results with a calibration curve obtained with liquid TBO samples of known concentration. A final density of 0.51 ± 0.24 nmol carboxyl groups per cm^2 was obtained, or 3 crosslinker molecules per nm^2, a very similar amount compared to the packing density measured in gold nanoparticles surfaces with the same molecule as measured by X-ray photoelectron spectroscopy.[26b] Considering the antibody as a smooth unhydrated sphere of mass M = 40,000 Da, its minimum radius (R_{min}) is calculated to be 2.25 nm following the equation (7),[39]

$$R_{min} = 0.066M^{1/3} \quad (7)$$

Final edited form was published in "Small: nano micro". 2019, 15 (23), S. 1-10. ISSN 1613-6829
https://doi.org/10.1002/smll.201901265

This allows the presence of maximum four antibodies per 100 nm^2 (two antibodies every 10 nm distance in both X and Y directions of the surface), meaning that the probability for them to find a surface carboxyl group is high (75 possible binding sites per antibody), leading to a surface fully covered by antibodies to ensure enough presence of functional biorecognition elements (maximum 2×10^8 antibodies in the total MoS_2 sensing area of 1×10^{10} nm^2).

The performance of the device as a biosensor was tested by comparing the output characteristics in dry state before and after the incubation of solutions with increasing VP40 concentrations (range: fM-nM). A drop of 20 µL PBS with target protein was deposited on top of the sensing area and incubated for 30 min. Then, PBS was used for rinsing, followed by a further rinse using 10 fold diluted PBS to remove excess of salts from the surface. The chip was dried using N_2 and the output characteristics were obtained. The results were compared with those obtained using staphylococcal enterotoxin B (SEB) as analyte, which shows initial symptoms similar to Ebola disease if ingested. Additionally, a control experiment was done detecting VP40 with a sensor lacking antibodies.

In the smallest tested concentration (2 fM), 2.4×10^4 molecules are present in the 20 µL droplet. Out of this number, only the ones at the MoS_2 deposited area will cause a signal change on the sensor. This amount can be estimated considering the ratio between the MoS_2 area and the area occupied by the sample droplet (1×10^4 $\mu m^2/9 \times 10^6$ $\mu m^2 = 1.1 \times 10^{-3}$), which multiplying to the total number of molecules results in the maximum number of antigens settled on the sensing area (2.1×10^7). This number is

Final edited form was published in "Small: nano micro". 2019, 15 (23), S. 1-10. ISSN 1613-6829
https://doi.org/10.1002/smll.201901265

one order of magnitude below the amount of antibodies previously calculated, allowing to perform the detection without reaching a saturation. Furthermore, each antibody could be recognizing more than one antigen, allowing to detect also higher concentrations. However, for a sample with 2 pM concentration, there will be a maximum of 2.4×10^{10} antigens to be detected on the sensing area, explaining the saturation of the signal at this point (Figure 3f).

A regeneration experiment was also carried out by repeating the same biosensing procedure on a biofunctionalized chip, followed by an incubation in regeneration buffer (10 mM glycine pH = 2 and 10% v/v glycerol) to separate the antigen from the antibody, and repeating the detection again.

Real samples were finally analyzed, consisting in fetal bovine serum samples with spiked VP40 protein.

Materials Characterization: X-ray diffraction (XRD) patterns were recorded on an X-ray diffractometer (D/max-2200/PC, Rigaku) using Cu-Kα radiation (λ = 0.15418 nm) at 40 kV. The scanning electron microscopy (SEM) and the transmission electron microscopy (TEM) images were recorded on a field emission scanning electron microscope (FESEM, Zeiss Gemini 500) and a high-resolution transmission electron microscope (HRTEM, JEM-2100, JEOL, Japan), respectively. Atomic force microscopy (AFM) characterization was carried out with Bruker Multimode 8 system for Figure 2d,e and Digital Instruments MMAFM-2 for Figure 3b-iv. Raman analysis was performed by using a Raman spectrometer (Renishaw inVia, 532 nm) at room temperature. UV-vis absorption spectra were measured in absorbance mode in a Jasco

Final edited form was published in "Small: nano micro". 2019, 15 (23), S. 1-10. ISSN 1613-6829
https://doi.org/10.1002/smll.201901265

V-570 spectrophotometer. The X-ray photoelectron spectroscopy (XPS) spectra were acquired using a Kratos Axis UltraDLD spectrometer (Kratos Analytical-A Shimadzu Group Company) with a monochromatic Al-Kα source (1486.6 eV).

Supporting Information

Supporting Information is available from the Wiley Online Library or from the author.

Acknowledgements

P.Z., S.Y, R.P.-G and B.I. contributed equally to this work. The authors thank the financial support from the German Research Foundation (DFG) within the Cluster of Excellence 'Center for Advancing Electronics Dresden' (cfaed) and the Initiative and Networking Fund of the German Helmholtz Association, Helmholtz International Research School for Nanoelectronic Networks NanoNet (VH-KO-606), Hamburg Science Award, ERC Grant on 2DMATER, HIPER-G, and EU Graphene Flagship. We also thank Dr. Xiaodong Zhuang (TUD), Dr. Jian Zhang (TUD), and Wenbo Sheng (TUD) for helpful discussions and characterizations. S. Y. acknowledges the funding from China Scholarship Council (CSC). We acknowledge the use of the facilities in the Dresden Center for Nanoanalysis at the Technische Universität Dresden.

Received: ((will be filled in by the editorial staff))
Revised: ((will be filled in by the editorial staff))
Published online: ((will be filled in by the editorial staff))

References

[1] G. Fiori, F. Bonaccorso, G. Iannaccone, T. Palacios, D. Neumaier, A. Seabaugh, S. K. Banerjee, L. Colombo, *Nat. Nanotechnol.* **2014**, *9*, 768.

[2] a) Q. H. Wang, K. Kalantar-Zadeh, A. Kis, J. N. Coleman, M. S. Strano, *Nat. Nanotechnol.* **2012**, *7*, 699; b) B. Radisavljevic, A. Radenovic, J. Brivio, V. Giacometti, A. Kis, *Nat. Nanotechnol.* **2011**, *6*, 147.

[3] a) Z. Yin, H. Li, H. Li, L. Jiang, Y. Shi, Y. Sun, G. Lu, Q. Zhang, X. Chen, H. Zhang, *ACS Nano* **2012**, *6*, 74; b) O. Lopez-Sanchez, D. Lembke, M. Kayci, A. Radenovic, A. Kis, *Nat. Nanotechnol.* **2013**, *8*, 497; c) Z. Sun, H. Chang, *ACS Nano* **2014**, *8*, 4133.

[4] a) A. Ambrosi, Z. Sofer, J. Luxa, M. Pumera, *ACS Nano* **2016**, *10*, 11442; b) S. S. Hong, W. Kundhikanjana, J. J. Cha, K. Lai, D. Kong, S. Meister, M. A. Kelly, Z.-X. Shen, Y. Cui, *Nano Lett.* **2010**, *10*, 3118.

[5] a) K. Lee, R. Gatensby, N. McEvoy, T. Hallam, G. S. Duesberg, *Adv. Mater.* **2013**, *25*, 6699; b) W. Zhang, P. Zhang, Z. Su, G. Wei, *Nanoscale* **2015**, *7*, 18364; c) X. Zhao, Y. Li, Y. Guo, Y. Chen, Z. Su, P. Zhang, *Adv. Mater. Interfaces* **2016**, *3*, 1600658.

[6] a) N. Choudhary, M. Patel, Y.-H. Ho, N. B. Dahotre, W. Lee, J. Y. Hwang, W.

Final edited form was published in "Small: nano micro". 2019, 15 (23), S. 1-10. ISSN 1613-6829
https://doi.org/10.1002/smll.201901265

Choi, *J. Mater. Chem. A* **2015**, *3*, 24049; b) P. Zhang, X. Lu, Y. Huang, J. Deng, L. Zhang, F. Ding, Z. Su, G. Wei, O. G. Schmidt, *J. Mater. Chem. A* **2015**, *3*, 14562.

[7] C. Ahn, J. Lee, H.-U. Kim, H. Bark, M. Jeon, G. H. Ryu, Z. Lee, G. Y. Yeom, K. Kim, J. Jung, Y. Kim, C. Lee, T. Kim, *Adv. Mater.* **2015**, *27*, 5223.

[8] X. Zhang, Z. Lai, C. Tan, H. Zhang, *Angew. Chem. Int. Ed.* **2016**, *55*, 8816.

[9] Z. Zeng, Z. Yin, X. Huang, H. Li, Q. He, G. Lu, F. Boey, H. Zhang, *Angew. Chem. Int. Ed.* **2011**, *50*, 11093.

[10] a) J. N. Coleman, M. Lotya, A. O'Neill, S. D. Bergin, P. J. King, U. Khan, K. Young, A. Gaucher, S. De, R. J. Smith, I. V. Shvets, S. K. Arora, G. Stanton, H.-Y. Kim, K. Lee, G. T. Kim, G. S. Duesberg, T. Hallam, J. J. Boland, J. J. Wang, J. F. Donegan, J. C. Grunlan, G. Moriarty, A. Shmeliov, R. J. Nicholls, J. M. Perkins, E. M. Grieveson, K. Theuwissen, D. W. McComb, P. D. Nellist, V. Nicolosi, *Science* **2011**, *331*, 568; b) V. Nicolosi, M. Chhowalla, M. G. Kanatzidis, M. S. Strano, J. N. Coleman, *Science* **2013**, *340*, 1226419.

[11] a) G. Cunningham, M. Lotya, C. S. Cucinotta, S. Sanvito, S. D. Bergin, R. Menzel, M. S. P. Shaffer, J. N. Coleman, *ACS Nano* **2012**, *6*, 3468; b) Y. Liu, X. He, D. Hanlon, A. Harvey, J. N. Coleman, Y. Li, *ACS Nano* **2016**, *10*, 8821.

[12] A. O'Neill, U. Khan, J. N. Coleman, *Chem. Mater.* **2012**, *24*, 2414.

[13] A. J. Cooper, M. Velický, I. A. Kinloch, R. A. W. Dryfe, *J. Electroanal. Chem.* **2014**, *730*, 34.

[14] W. Sirisaksoontorn, A. A. Adenuga, V. T. Remcho, M. M. Lerner, *J. Am. Chem. Soc.* **2011**, *133*, 12436.

[15] C. E. Dahm, D. G. Peters, *J. Electroanal. Chem.* **1996**, *402*, 91.

[16] a) N. Liu, P. Kim, J. H. Kim, J. H. Ye, S. Kim, C. J. Lee, *ACS Nano* **2014**, *8*, 6902; b) F. Wypych, C. Solenthaler, R. Prins, T. Weber, *J. Solid State Chem.* **1999**, *144*, 430.

[17] W. M. R. Divigalpitiya, S. R. Morrison, R. F. Frindt, *Thin Solid Films* **1990**, *186*, 177.

[18] A. Kozbial, X. Gong, H. Liu, L. Li, *Langmuir* **2015**, *31*, 8429.

[19] G. Schwartz, B. C. K. Tee, J. Mei, A. L. Appleton, D. H. Kim, H. Wang, Z. Bao, *Nat. Commun.* **2013**, *4*, 1859.

[20] a) G.-H. Lee, Y.-J. Yu, X. Cui, N. Petrone, C.-H. Lee, M. S. Choi, D.-Y. Lee, C. Lee, W. J. Yoo, K. Watanabe, T. Taniguchi, C. Nuckolls, P. Kim, J. Hone, *ACS Nano* **2013**, *7*, 7931; b) J. Yoon, W. Park, G.-Y. Bae, Y. Kim, H. S. Jang, Y. Hyun, S. K. Lim, Y. H. Kahng, W.-K. Hong, B. H. Lee, H. C. Ko, *Small* **2013**, *9*, 3295; c) R. Cheng, S. Jiang, Y. Chen, Y. Liu, N. Weiss, H.-C. Cheng, H. Wu, Y. Huang, X. Duan, *Nat. Commun.* **2014**, *5*, 5143; d) B. Ryu, E. Yang, Y. Park, K. Kurabayashi, X. Liang, *J. Vac. Sci. Technol. B* **2017**, *35*, 06G805; e) G. A. Salvatore, N. Münzenrieder, C. Barraud, L. Petti, C. Zysset, L. Büthe, K. Ensslin, G. Tröster, *ACS Nano* **2013**, *7*, 8809.

[21] a) D. De Fazio, I. Goykhman, D. Yoon, M. Bruna, A. Eiden, S. Milana, U. Sassi, M. Barbone, D. Dumcenco, K. Marinov, A. Kis, A. C. Ferrari, *ACS Nano* **2016**, *10*, 8252; b) M.-A. Kang, S. J. Kim, W. Song, S.-j. Chang, C.-Y. Park, S. Myung,

Final edited form was published in "Small: nano micro". 2019, 15 (23), S. 1-10. ISSN 1613-6829
https://doi.org/10.1002/smll.201901265

J. Lim, S. S. Lee, K.-S. An, *Carbon* **2017**, *116*, 167.

[22] D. Karnaushenko, B. Ibarlucea, S. Lee, G. Lin, L. Baraban, S. Pregl, M. Melzer, D. Makarov, W. M. Weber, T. Mikolajick, O. G. Schmidt, G. Cuniberti, *Adv. Healthcare Mater.* **2015**, *4*, 1517.

[23] Z. Wang, M. Shaygan, M. Otto, D. Schall, D. Neumaier, *Nanoscale* **2016**, *8*, 7683.

[24] N. R. Shanmugam, S. Muthukumar, S. Prasad, *Sci. Rep.* **2016**, *6*, 33423.

[25] S. Presolski, M. Pumera, *Mater. Today* **2016**, *19*, 140.

[26] a) C. Chollet, C. Chanseau, B. Brouillaud, M. C. Durrieu, *Biomol. Eng.* **2007**, *24*, 477; b) M. R. Ivanov, A. J. Haes, *Anal. Chem.* **2012**, *84*, 1320.

[27] M. A. Cooper, D. H. Williams, *Anal. Biochem.* **1999**, *276*, 36.

[28] a) D. Sarkar, W. Liu, X. Xie, A. C. Anselmo, S. Mitragotri, K. Banerjee, *ACS Nano* **2014**, *8*, 3992; b) J. Lee, P. Dak, Y. Lee, H. Park, W. Choi, M. A. Alam, S. Kim, *Sci. Rep.* **2014**, *4*, 7352.

[29] A. Kaushik, S. Tiwari, R. Dev Jayant, A. Marty, M. Nair, *Biosens. Bioelectron.* **2016**, *75*, 254.

[30] B. Ibarlucea, T. Fawzul Akbar, K. Kim, T. Rim, C.-K. Baek, A. Ascoli, R. Tetzlaff, L. Baraban, G. Cuniberti, *Nano Res.* **2018**, *11*, 1057.

[31] E. D. Grayfer, A. S. Nazarov, V. G. Makotchenko, S.-J. Kim, V. E. Fedorov, *J. Mater. Chem.* **2011**, *21*, 3410.

[32] W. Lv, M. Guo, M.-H. Liang, F.-M. Jin, L. Cui, L. Zhi, Q.-H. Yang, *J. Mater. Chem.* **2010**, *20*, 6668.

[33] a) B. Ibarlucea, T. Rim, C. K. Baek, J. A. G. M. de Visser, L. Baraban, G. Cuniberti, *Lab Chip* **2017**, *17*, 4283; b) D. M. Kim, Y.-H. Jeong, *Nanowire Field Effect Transistors: Principles and Applications*, Springer, **2014**.

[34] J. Schütt, B. Ibarlucea, R. Illing, F. Zörgiebel, S. Pregl, D. Nozaki, W. M. Weber, T. Mikolajick, L. Baraban, G. Cuniberti, *Nano Lett.* **2016**, *16*, 4991.

[35] E. Baek, T. Rim, J. Schütt, C.-k. Baek, K. Kim, L. Baraban, G. Cuniberti, *Nano Lett.* **2017**, *17*, 6727.

[36] S. Y. Xiao, L. F. Che, X. X. Li, Y. L. Wang, *Microelectron. Eng.* **2008**, *85*, 452.

[37] C. E. Carraher Jr, *Carraher's polymer chemistry*, CRC Press, Taylor & Francis Group, USA **2016**.

[38] a) H. Fang, K. J. Yu, C. Gloschat, Z. Yang, E. Song, C.-H. Chiang, J. Zhao, S. M. Won, S. Xu, M. Trumpis, Y. Zhong, S. W. Han, Y. Xue, D. Xu, S. W. Choi, G. Cauwenberghs, M. Kay, Y. Huang, J. Viventi, I. R. Efimov, J. A. Rogers, *Nat. Biomed. Eng.* **2017**, *1*, 0038; b) Y.-T. Chang, J.-H. Huang, M.-C. Tu, P. Chang, T.-R. Yew, *Biosens. Bioelectron.* **2013**, *41*, 898.

[39] H. P. Erickson, *Biol. Proced. Online* **2009**, *11*, 32.

[40] G. Yoo, H. Park, M. Kim, W. G. Song, S. Jeong, M. H. Kim, H. Lee, S. W. Lee, Y. K. Hong, M. G. Lee, S. Lee, S. Kim, *Nano Res.* **2017**, *10*, 767.

[41] D. Kinnamon, R. Ghanta, K.-C. Lin, S. Muthukumar, S. Prasad, *Sci. Rep.* **2017**, *7*, 13312.

[42] D.-W. Lee, J. Lee, I. Y. Sohn, B.-Y. Kim, Y. M. Son, H. Bark, J. Jung, M. Choi, T. H. Kim, C. Lee, N.-E. Lee, *Nano Res.* **2015**, *8*, 2340.

Final edited form was published in "Small: nano micro". 2019, 15 (23), S. 1-10. ISSN 1613-6829
https://doi.org/10.1002/smll.201901265

Final edited form was published in "Small: nano micro". 2019, 15 (23), S. 1-10. ISSN 1613-6829
https://doi.org/10.1002/smll.201901265

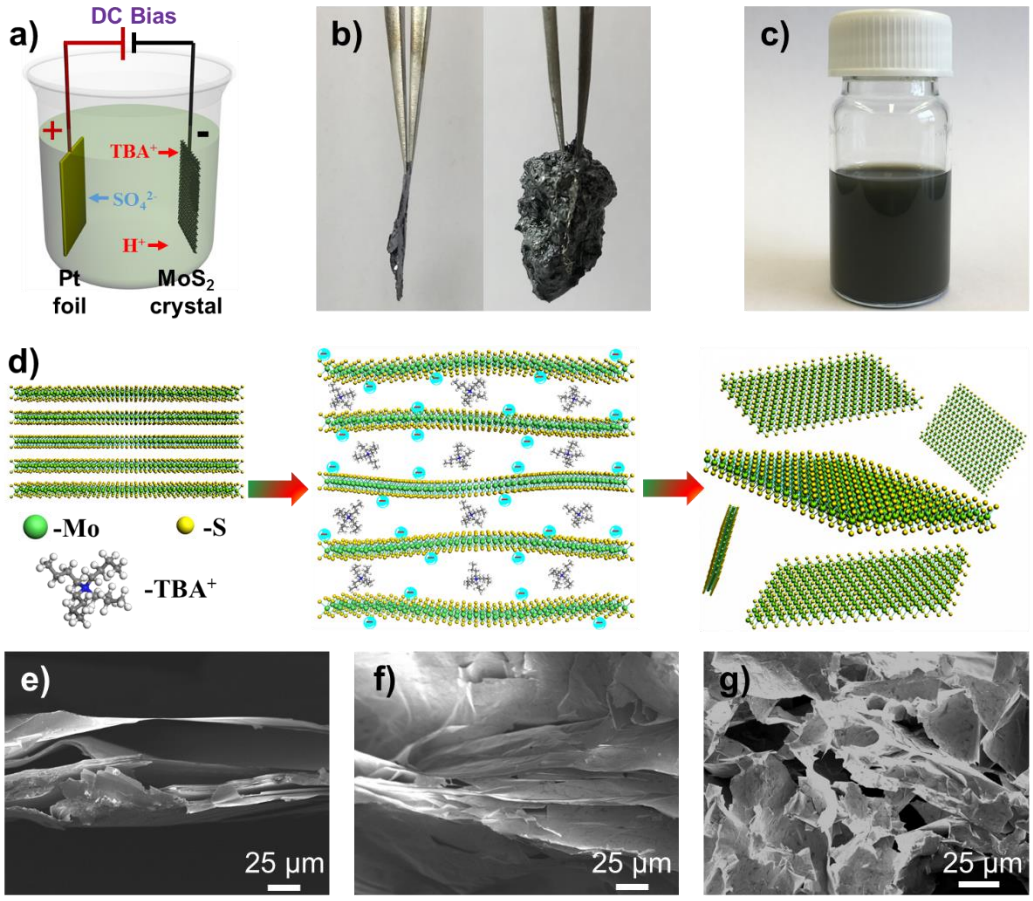

Figure 1. Electrochemical exfoliation of MoS_2 flakes: a) schematic illustration of an electrochemical exfoliation cell, b) photographs of bulk MoS_2 crystal (left) and expand MoS_2 crystal after exfoliation (right), c) MoS_2 flakes dispersed in propylene carbonate, d) schematic illustration for mechanism of electrochemical exfoliation, and e-g) SEM images of MoS_2 crystal at the edges after applying a bias of -5 V for 0, 1 and 10 min in organic TBA▪HSO_4 electrolyte, respectively.

Final edited form was published in "Small: nano micro". 2019, 15 (23), S. 1-10. ISSN 1613-6829
https://doi.org/10.1002/smll.201901265

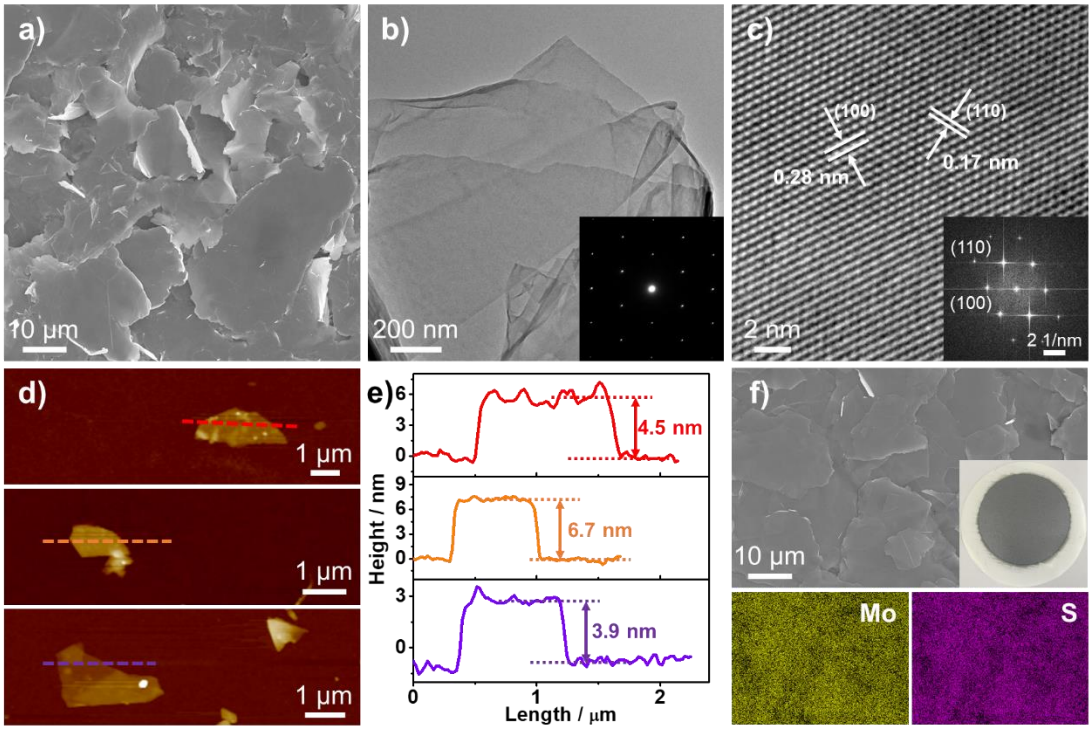

Figure 2. Morphological characterizations of exfoliated MoS_2 flakes and thin film. a) SEM image of exfoliated MoS_2 flakes on Si/SiO_2 wafer, b, c) HR-TEM images and corresponding diffraction patterns (inset) of a few-layered MoS_2 flake, d) AFM images and e) height profiles of exfoliated MoS_2 flakes taken from the supernatant, and f) top-view SEM image of MoS_2 thin film and corresponding EDS elemental mapping analysis. Inset: Photograph of MoS_2 thin film on a PTFE membrane (50 mm in diameter).

Final edited form was published in "Small: nano micro". 2019, 15 (23), S. 1-10. ISSN 1613-6829
https://doi.org/10.1002/smll.201901265

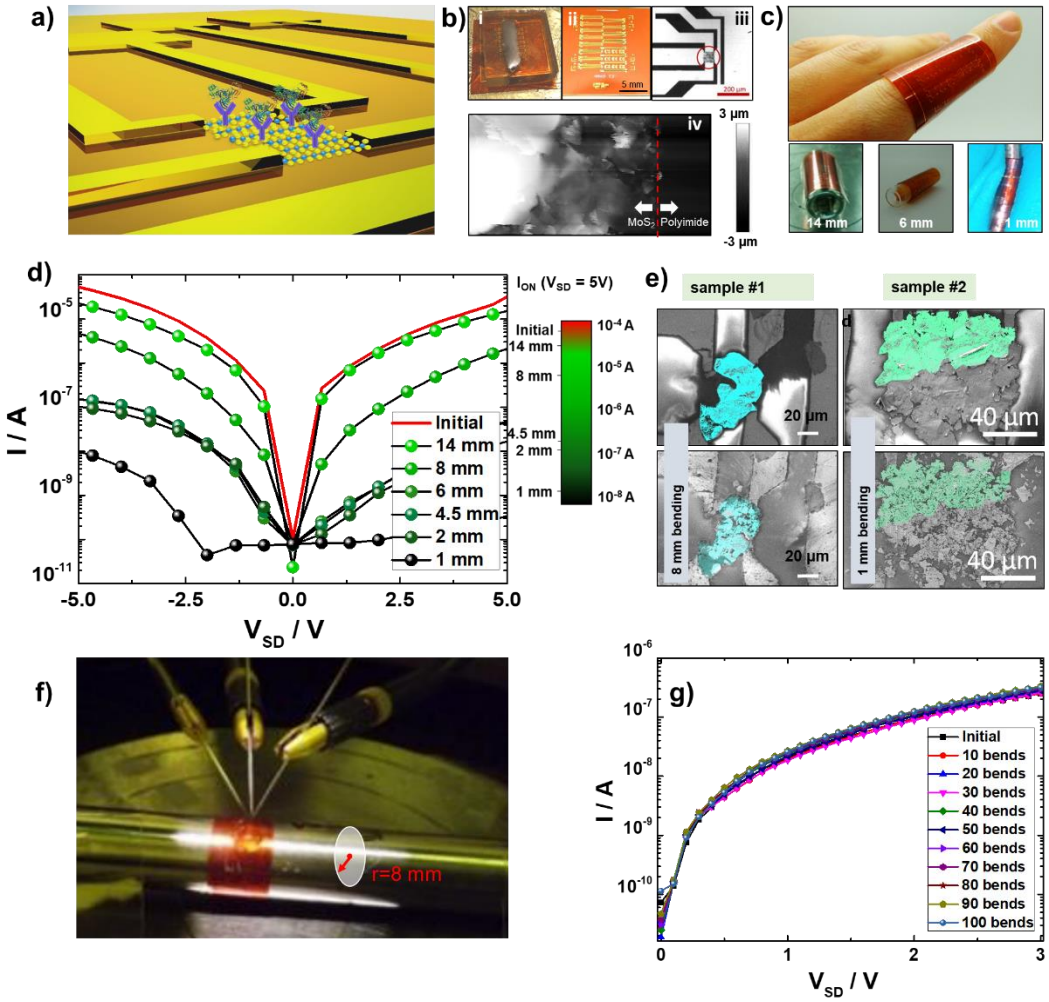

Figure 3. a) Conceptual illustration of the biosensing. b) Images of fabrication process. i: photography of the floating MoS_2 layer; ii: fabricated device containing several sensors; iii: magnification of one single sensor with deposited MoS_2 layer (60 × 60 µm) contacting four electrodes; iv: AFM image of the MoS_2 layer. c) Fabricated flexible device bended at various radius, including the 14 mm, 8 mm and 1 mm from the bending test. d) Bending test, including initial output characteristics before bending (red curve). The lateral panel shows the I_{ON} at V_{SD} = -5 V upon various bending radii. e) SEM images before (top panels) and after (bottom panels) bending at 8 mm (left panels) and 1 mm radius (right panels). The possible conductive paths connecting electrodes are shown in color. f) Setup for the cyclic test with the flexible chip bent at the 8 mm radius cylinder. g) Results of the cyclic bending test, with no visible change after 100 bending cycles.

Final edited form was published in "Small: nano micro". 2019, 15 (23), S. 1-10. ISSN 1613-6829
https://doi.org/10.1002/smll.201901265

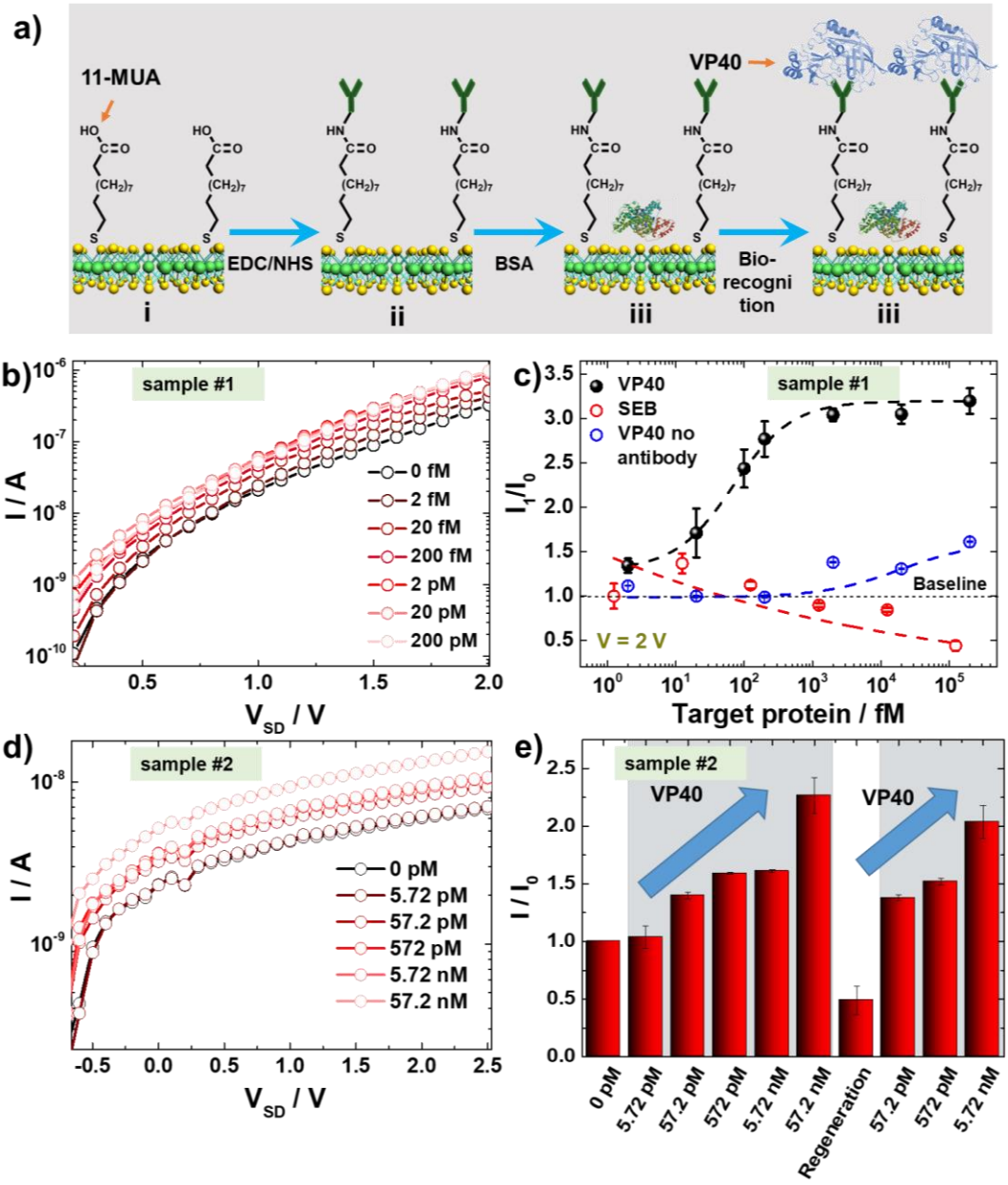

Figure 4. a) Biofunctionalization steps: i) 11-MUA incorporation on sulfur vacancies; ii) Antibody immobilization through carbodiimide chemistry; iii) Surface blocking with BSA; iv) Biorecognition of VP40 antigen. b) Current measurements after the incubation of various antigen concentrations on a sensor with a high amount of flakes, and c) calibration of the response and comparison with control sensors (no antibody and non-specific antigen). d) Repetition of the biosensing experiment on a sensor with a lower amount of flakes and e) results of the regeneration experiment with the same device, showing signal recovery after antibody-antigen dissociation and repetition of the tendency after further analyte incubation.

Final edited form was published in "Small: nano micro". 2019, 15 (23), S. 1-10. ISSN 1613-6829
https://doi.org/10.1002/smll.201901265

Table 1. Comparative table for various MoS_2-based biosensors.

MoS_2 material	**Deposition**	**Sensing area**	**Lowest detection**	**Flexibility**	**Ref.**
Prebent MoS_2 (undefined obtention method)	Transfer-printing	5×10 µm	10 fM interleukin 1-beta	0.1/mm	[20d]
Mechanically exfoliated MoS_2	Transfer (undescribed)	Variable	33 fM prostate specific antigen	3 mm	[40]
Chemically exfoliated MoS_2	Vacuum assisted dispersion through membrane	Undefined, multiple flakes embedded on 110 µm thick membrane	2.76 nM cortisol	5 mm	[41]
Mechanically exfoliated MoS_2	Electrode deposition on exfoliated flakes	Variable	100 fM streptavidin	Not tested	[28a]
Direct sulfurization of Mo surface	Evaporated Mo metal through shadow mask	300×6,000 µm	10 fM ssDNA (18-mer)	Not flexible	[42]
Electrochemically exfoliated MoS_2	Restacking of the flakes at the PI substrate	80×80 µm	2 fM	1 mm	This work